Int. J. Multiphase Flow Vol. 18, No. 5, pp. 751–764, 1992
Printed in Great Britain.

0301-9322/92 $5.00 + 0.00

HYDRODYNAMIC INTERACTIONS BETWEEN TWO SPHERES NEAR A SOLID PLANE

T. DABROS† and T. G. M. VAN DE VEN
Paprican and Department of Chemistry, Pulp and Paper Research Centre, McGill University, Montreal, Quebec, Canada H3A 2A7

(Received 4 December 1990; in revised form 14 May 1992)

Abstract—Hydrodynamic interactions between particles deposited on a solid wall and those free to move in a simple shear or a stagnation point flow were studied by the boundary element method. There are two effects which can play an important role during deposition, namely: (i) disturbance of the particle trajectories by the deposited particles; and (ii) an extra hydrodynamic force on a deposited particle during a two-body encounter. The first effect slows down the deposition rate on the collector surface (blocking), while the second effect can increase particle removal from the surface. We have shown that hydrodynamic effects cannot explain the large blocking effects commonly observed; these must be due to colloidal interactions, not included in this paper. However, the force exerted on a deposited particle can be changed considerably when a second particle collides with it under purely hydrodynamic conditions. This effect is likely to be responsible for the removal of weakly-bound particles.

Key Words: hydrodynamic interactions, particle deposition, particle removal, two-sphere interactions

INTRODUCTION

The problem of the motion of colloidal particles through a viscous fluid has, over the years, received a great deal of attention. This paper deals with problems related to particle deposition on surfaces and addresses the problem of non-linear kinetics, which is still poorly understood. However, some results may be of interest for the analysis of rheological properties, epecially in the wall region of a suspension.

It is widely accepted that the motion of colloidal particles is governed by the linearized steady-state Navier–Stokes equations. The fluid is assumed to be incompressible and Newtonian. But even adopting these simplifications, the equations have been solved in an analytical manner for only a limited number of systems with simple geometries. The famous Stokes (1851) solution for a sphere in a uniform flow is an example. Other solved problems of low Reynolds hydrodynamics are extensively discussed in books by Happel & Brenner (1965) and van de Ven (1989). Progress in the analysis of the flow equtions for a single sphere in the vicinity of a solid wall made it possible to calculate the flux of colloidal particles to a variety of collectors, such as the rotating disk (Spielman & Fitzpatrick 1973; Dabros *et al.* 1977; Dabros & Adamczyk 1979), the spherical collector (Prieve & Ruckenstein 1974; Adamczyk & van de Ven 1981b) and flat and cylindrical channels (Bowen & Epstein 1979; Adamczyk & van de Ven 1981a etc.).

The theoretical predictions were tested experimentally and, in many cases, a satisfactory agreement was noted (Dabros & van de Ven 1983; Adamczyk 1989a, b). However, it should be borne in mind, that the theory neglects interparticle interactions of any kind, not only in the solution, but also in the interface region. It can be shown that for a sufficiently dilute dispersion, when particle–particle interactions in the bulk are negligible, interactions between flowing and deposited particles in the interface region can still be significant, even for small coating densities. In other words, the dispersion near the interface is no longer "dilute".

Interactions between deposited and flowing particles are responsible for all kinds of blocking effects and structuring of the deposit (Adamczyk 1989a, b). The description of hydrodynamic two-sphere interactions near an interface is in its early stage of development. In recent years a number of numerical techniques have been suggested to deal with related problems, the most

†On leave from Jagiellonian University, Krakow, Poland.

important ones being: (i) the method of reflections; (ii) the boundary collocation truncated series solution; (iii) the finite element method; (iv) the singularity method; (v) the boundary element method (BEM); and (vi) the multisubunit method. A short review of the first five methods can be found in a recent paper by Hsu & Gantos (1989) and Weinbaum *et al.* (1990). The multisubunit method was used by Dabros (1989) to study interactions between particles during the deposition process at a stagnation point flow collector. Youngren & Acrivos (1975) used the integral equation to calculate hydrodynamic forces and torques acting on spheroidal and cylindrical particles in a uniform and simple shear flow in an unbounded fluid. The surface of the body was divided into elements in each of which the Stokeslets strength was assumed to be constant. By these means the problem was reduced to a system of linear algebraic equations with unknown Stokeslets distributions.

Dabros (1985) developed a singularity method based on singular forces and sources situated inside each particle. The strength of the singularities was determined from the no-slip boundary conditions on the particle surface.

Other techniques, based on a representation of the Stokeslets distribution by a double series are discussed by Hsu & Gantos (1989), where the method was used to calculate the hydrodynamic force and torque on an arbitrary body of revolution in the vicinity of a solid wall. An excellent survey of recent advances in numerical techniques for solving many-body problems is the book by Kim & Karrila (1991).

We decided to use a BEM similar to the one used to solve many engineering problems (Brebbia *et al.* 1980; Beskos 1987). This method is conceptually simple and complements other techniques for solving Stokes flow problems with many-body interactions. Its major advantage is that, for the problem of two-sphere interactions near a wall, one can make use of the analytical form of the Oseen tensor for a point force near a plane which satisfies the no-slip boundary condition. Since only the surfaces of the spheres require discretization, a reduction in the spatial dimension of the problem results. A disadvantage of the method is related to the characteristic feature of the influence matrix which arises in this method. This matrix is, in general, non-symmetric and fully populated, making the use of special techniques available for symmetric or sparse matrices impossible.

The aim of the paper is two-fold. In the first place, we are interested in the non-linear deposition kinetics frequently observed in deposition experiments. This is believed to be due to particle interactions at the surface which interfere with the deposition process and can result in particle detachment. Secondly, we are interested in effective ways of numerically solving hydrodynamic many-body problems near a solid boundary.

METHOD

In our analysis we adopted the linearized, steady-state Navier–Stokes equation (creeping flow equation), which will describe the flow of a Newtonian, incompressible fluid:

$$\mu \nabla^2 \mathbf{v} = \nabla p \qquad [1]$$

and

$$\nabla \cdot \mathbf{v} = 0, \qquad [2]$$

where $\mathbf{v}(\mathbf{x})$ is the fluid flow velocity at point $\mathbf{x}$, μ is the dynamic viscosity of the fluid and p is the pressure. We will study the zero Reynolds number (Re) hydrodynamic interactions between two similar spherical particles of radius a. Let us consider the case when the system is bounded by a stationary solid surface W and let $\mathbf{v}^0(\mathbf{x})$ denote the fluid flow field in the absence of the particles. The velocity $\mathbf{v}^0(\mathbf{x})$ itself has to fulfill [1] and [2] with the no-slip boundary conditions on W.

The Green's function $G(\mathbf{x}, \mathbf{y})$ for the problem will hereafter be called the Oseen tensor. The Oseen tensor is assumed to satisfy the boundary conditions $G(\mathbf{x}, \mathbf{y}) = 0$ for $\mathbf{x} \in W$. The wall W is chosen to coincide with the plane $z = 0$. For such a case, the Oseen tensor can be expressed as the sum of two terms

$$G(\mathbf{x}, \mathbf{y}) = G^0(\mathbf{x}, \mathbf{y}) + G^W(\mathbf{x}, \mathbf{y}) \qquad [3]$$

where $G^0(\mathbf{x}, \mathbf{y})$ has the following components:

$$G^0_{ij}(\mathbf{x}, \mathbf{y}) = \frac{1}{8\pi\mu r}\left(\delta_{ij} + \frac{r_i r_j}{r^2}\right), \qquad [4]$$

where $\mathbf{r} = \mathbf{x} - \mathbf{y}$, r_i are components of $\mathbf{r}$ and $r = |\mathbf{r}|$; δ_{ij} is the Kronecker unit tensor. Thus, $G^0(\mathbf{x}, \mathbf{y})$ is the ordinary Oseen tensor for an unbounded fluid (Oseen 1927). It should be noted that the tensor $G^0(\mathbf{x}, \mathbf{y}) = G^0(\mathbf{x} - \mathbf{y})$ has a singularity as $r \to 0$.

The second term on the right-hand side of [3] can be considered as originating from the image system of force and source singularities which account for the presence of the wall in order to fulfill the boundary conditions. It has been shown by Blake (1971), that $G^W(\mathbf{x}, \mathbf{y})$ has the following components:

$$G^W_{ij}(\mathbf{x}, \mathbf{y}) = \frac{1}{8\pi\mu r^*}\left\{-\left(\delta_{ij} + \frac{r_i^* r_j^*}{r^{*2}}\right) + 2hr^* J_{jk}\frac{\partial}{\partial r_k^*}\left[\frac{hr_i^*}{r^{*3}} - \left(\frac{\delta_{i3}}{r^*} + \frac{r_i^* r_3^*}{r^{*3}}\right)\right]\right\}, \qquad [5]$$

where $J_{jk} = (\delta_{jk} - 2\delta_{j3}\delta_{k3})$ is the reflection tensor (w.r.t the plane $z = 0$). The vector $\mathbf{r}^*$ has components r_i^* equal to $(x_1 - y_1, x_2 - y_2, x_3 + y_3)$, $r^* = |\mathbf{r}^*|$ and $h = y_3$.

The integral solution of the Stokes equation, appropriate for the case of two solid particles under consideration, takes the form:

$$\mathbf{v}(\mathbf{x}) = \mathbf{v}^0(\mathbf{x}) + \sum_{l=1}^{2}\int_{S_l} G(\mathbf{x}, \mathbf{y})\cdot\mathbf{f}(\mathbf{y})\,\mathrm{d}S_y. \qquad [6]$$

In this formula $\mathbf{y}$ is a vector pointing to the surface element $\mathrm{d}S_y$, $\mathbf{f}(\mathbf{y})$ is the force density at $\mathbf{y}$ and S_l is the surface of particle $l (l = 1, 2)$.

The total force $\mathbf{F}_l$ and torque $\mathbf{T}_l$ exerted by particle l on the fluid are given by the equations:

$$\mathbf{F}_l = \int_{S_l} \mathbf{f}(\mathbf{y})\,\mathrm{d}S_y \qquad [7]$$

and

$$\mathbf{T}_l = \int_{S_l} (\mathbf{y} - \mathbf{R}_l) \times \mathbf{f}(\mathbf{y})\,\mathrm{d}S_y, \qquad [8]$$

where $\mathbf{R}_l$ specifies the position of the center of particle l.

In order to obtain a closed system of equations one must take into account the boundary conditions at the particle surface:

$$\mathbf{v}(\mathbf{x}) = \mathbf{u}(\mathbf{x}) \quad \text{for } \mathbf{x} \in S_l. \qquad [9]$$

The velocity of the surface point $\mathbf{x}$ of solid particle l can be expressed as

$$\mathbf{u}(\mathbf{x}) = \mathbf{u}_l + \boldsymbol{\Omega}_l \times (\mathbf{x} - \mathbf{R}_l), \qquad [10]$$

where $\mathbf{u}_l$ and $\boldsymbol{\Omega}_l$ are the translational and rotational velocities of particle l, respectively.

Equations [6]–[10] form a closed system of equations, provided that the external force and torque or the velocities of the particles are specified, as well as the external velocity flow field $\mathbf{v}^0(\mathbf{x})$.

THE BOUNDARY ELEMENT METHOD (BEM)

Let us assume that the surface of each particle is divided into M_e triangular elements in such a way that the surface elements do not overlap and all points of the sides of the triangles coincide with the sphere surface. We will assume that the two considered spherical particles are discretized in a similar way. The surface integrals in [6]–[10] can be expressed by the sums of the integrals over the elements. Taking into account the boundary condition [10], one obtains

$$\mathbf{u}_l + \boldsymbol{\Omega}_l \times \mathbf{r}_l = \mathbf{v}^0(\mathbf{x}_l) + \sum_{k=1}^{2}\sum_{\beta=1}^{M_e}\int_{S_k^\beta} G(\mathbf{x}_l, \mathbf{y}_k^\beta)\cdot\mathbf{f}(\mathbf{y}_k^\beta)\,\mathrm{d}S_y, \qquad [11]$$

where $\mathbf{r}_l = \mathbf{x}_l - \mathbf{R}_l$, $\mathbf{x}_l$ and $\mathbf{y}_k^\beta$ are the surface points of the particles. Indexes l, $k = 1, 2$, while M_e is the number of elements on each surface.

In a similar way, the forces and torques can be expressed by

$$\mathbf{F}_l = \sum_{\beta=1}^{M_e} \int_{S_l^\beta} \mathbf{f}(\mathbf{y}_l^\beta)\, \mathrm{d}S_l \qquad [12]$$

and

$$\mathbf{T}_l = \sum_{\beta=1}^{M_e} \int_{S_l^\beta} [\mathbf{r}_l^\beta \times \mathbf{f}(\mathbf{y}_l^\beta)]\, \mathrm{d}S_y. \qquad [13]$$

In order to evaluate the surface integrals numerically a local coordinate system (ξ_1, ξ_2, ξ_3), rather than the global Cartesian system (x_1, x_2, x_3), is introduced. In the present paper we have adopted triangular elements with 6 nodal points; 3 of them in the corners of each triangle and 3 being midside points. The geometry of the system is described by the so-called shape functions $N^\alpha(\xi_1, \xi_2)$, which, in principle, are interpolation functions over an element α. The surface point $\mathbf{y}$ with Cartesian components $y_i (i = 1, 2, 3)$ can be expressed in terms of the nodal points $y_i^{\alpha\gamma}$ of a given surface element α (where $\gamma = 1, 2 \ldots 6$) and the shape functions in the following manner:

$$y_i = \sum_{\gamma=1}^{6} N^\gamma(\xi_1, \xi_2) y_i^{\alpha\gamma}. \qquad [14]$$

The six shape functions N^γ are given by

$$\begin{gathered} N^1 = \xi_1(2\xi_1 - 1), \quad N^2 = \xi_2(2\xi_2 - 1), \quad N^3 = \xi_3(2\xi_3 - 1), \\ N^4 = 4\xi_1\xi_3, \quad N^5 = 4\xi_1\xi_2, \quad N^6 = 4\xi_2\xi_3. \end{gathered} \qquad [15]$$

where $\xi_3 = 1 - \xi_1 - \xi_2$.

Similar to y_i, any field variable, e.g. $f_i^\beta(\mathbf{x})$, can be calculated inside the surface element β:

$$f_i^\beta(\mathbf{x}) = \sum_{\gamma=1}^{6} N^\gamma(\xi_1, \xi_2) f_i^{\beta\gamma}(\mathbf{x}(\xi_1, \xi_2)). \qquad [16]$$

The differentials of the surface $\mathrm{d}S$ can now be written as

$$\mathrm{d}S = |J|\, \mathrm{d}\xi_1\, \mathrm{d}\xi_2, \qquad [17]$$

where $|J| = (J_1^2 + J_2^2 + J_3^2)^{1/2}$ is the Jacobian of the transformation, which can be expressed in terms of the coordinates x_i and the local variables ξ_1, ξ_2:

$$\begin{aligned} J_1 &= \frac{\partial x_2}{\partial \xi_1}\frac{\partial x_3}{\partial \xi_2} - \frac{\partial x_3}{\partial \xi_1}\frac{\partial x_2}{\partial \xi_2}, \\ J_2 &= \frac{\partial x_3}{\partial \xi_1}\frac{\partial x_1}{\partial \xi_2} - \frac{\partial x_1}{\partial \xi_1}\frac{\partial x_3}{\partial \xi_2}, \\ J_3 &= \frac{\partial x_1}{\partial \xi_1}\frac{\partial x_2}{\partial \xi_2} - \frac{\partial x_2}{\partial \xi_1}\frac{\partial x_1}{\partial \xi_2}. \end{aligned} \qquad [18]$$

Integration in the local coordinate system can be performed in a convenient way using the standard Gaussian quadratature formulas (Brebbia *et al.* 1980). In the present paper we adopted 7- or 25-point formulas to integrate over element surfaces without singularities. If a singularity occurred a special integration formula was adopted, as described in Brebbia *et al.* (1980). In a number of test calculations it was found that, far away from the solid surface, no significant difference is noted if the number of integration points is changed from 7 to 25. However, in the wall region it was essential to apply the 25-point integration formula.

The discretization of the particle surfaces is shown in figure 1. We used 32 triangular surface elements defined by 6 nodal points in order to approximate the particle shape. The total number of nodal points $M = 66$. The surface area of the particle calculated numerically was approx. 0.7% smaller than the surface area of the original spheres, indicating the accuracy of the surface representation by the grid.

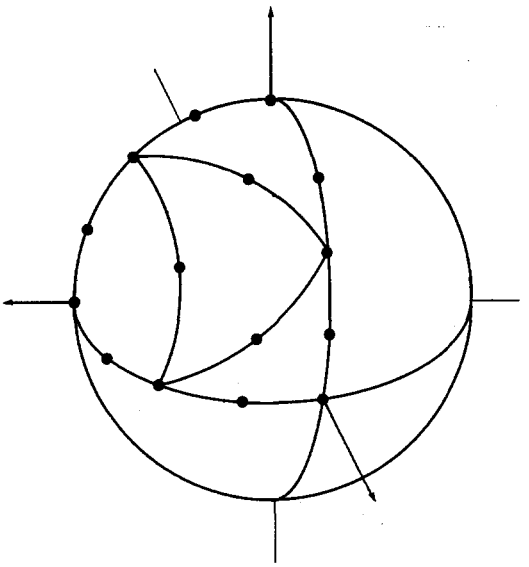

Figure 1. Discretization of the particle surface. The grid at one-quarter of the upper part of the sphere is shown.

For the purpose of interpolating the force density over the particle surface, all 66 points in test calculations and only 18 corner points of every triangle were used in most of the calculations, especially for two spheres. The lack of the side points increases the accuracy of the integrations in the latter case, so no essential differences were seen if the number of interpolation points was decreased.

Hereafter we will consider two identical spherical particles: one of them free to move and rotate due to the action of the external flow field, forces and torques; the second one will be stationary. Substitution of [14]–[17] into [11]–[13] result in a system of linear equations of the general form:

$$\mathbf{A} \cdot \mathbf{b} = \mathbf{c}. \qquad [19]$$

Here $\mathbf{A}$ is a matrix, the elements of which can be calculated on the basis of [11]–[13]. The vector $\mathbf{c}$ consists of known components corresponding to the external force and torque on the mobile particle and $6M$ components of the external flow velocity at the nodal points of the spheres. The unknown vector $\mathbf{b}$ includes $6M$ values of the force density at the nodal points of both particles and the 6 components of the translational and rotational velocity of the mobile particle. Details of the matrix $\mathbf{A}$ and vectors $\mathbf{c}$ and $\mathbf{b}$ can be found in the Appendix.

For the two-sphere problem under consideration and M nodal points, [19] is equivalent to a system of $6(M + 1)$ linear equations with the same number of unknowns. The standard Gaussian elimination method was used to solve the equations. This yields the 6 components of the translational and rotational velocity of the mobile particle, plus the force density $\mathbf{f}(\mathbf{y}_j^\beta)$ at each nodal point from which the forces and torques on the particles can be calculated from [12] and [13].

Before addressing the important problem of two spheres near a wall, we performed test calculations for one sphere near a wall and two spheres far from a wall, to ensure that the method works well in these two limits.

RESULTS

(a) Test Calculations for One Sphere Near a Wall

The test calculations show that the response of the sphere to a unit force in an infinite fluid is 0.8 and 0.5% higher than predicted by the Stokes formula for 66 and 18 nodal points, respectively. The response to a unit torque was up to 2% higher than expected from the exact solution of the Stokes equation. The deviations are due to imperfections in reproducing the particle shape and discretization errors during the numerical treatment of the problem.

Figure 2 shows the correction factor f_1 to the Stokes formula for the case when a single sphere of radius a approaches the solid wall perpendicularly. Defining the z-axis as normal to the wall, the force F_z exerted by the particle upon the fluid is given by

$$F_z = \frac{6\pi\mu a u_z}{f_1\left(\frac{h}{a}\right)}, \qquad [20]$$

where $h = z - a$.

The analytical solution of the problem given by Maude (1961) and Brenner (1961) is shown by the solid line. As one can see, good agreement exists between the solution calculated with the BEM and the exact solution for separations $>5\%$ of the particle radii. For this case it was noted that scatter in the results occurred for $h < 0.1$ if single precision arithmetic or low-order Gaussian quadrature was used in the calculations. The results shown hereafter will refer to calculations which were done with double precision and 25-point Gaussian quadrature.

Figure 3 shows the dependence of the normal component of the particle velocity u_z on h/a. The particle was placed in a stagnation point flow field:

$$\mathbf{v}^0(\mathbf{x}) = (\mathbf{i}Axz + \mathbf{j}Ayz - \mathbf{k}Az^2), \qquad [21]$$

where **i**, **j**, **k** are unit vectors of the Cartesian system of reference and A is a flow intensity parameter. The z-component of velocity is made dimensionless with respect to the fluid flow velocity $V_{\text{eff}} = -Az^2$. As was shown by Goren & O'Neill (1971), the ratio u_z/V_{eff} is a function of h/a only. Again, the solid line was calculated on the basis of the analytical solution of the Stokes equation (Goren & O'Neill 1971) and the points were calculated using the BEM. The ratio u_z/V_{eff}, by its very nature, depends on the friction forces of the sphere approaching the wall and on the hydrodynamic forces exerted on a stationary particle by the flow field at a given position. Thus, it is not striking that the accuracy of these calculations increases in the same region as those presented in figure 2. In order to complete the data on the performance of the method in a stagnation point flow, in figure 4 one can see the dependence of the dimensionless coefficient $f_2(h/a)$ to the Stokes formula for the normal force exerted by the fluid on a stationary sphere with its center at distance z from the wall. These results, as well as others done for simple shear flow and movement of the particle tangential to the wall, show that the error of the calculations becomes significant at separations $<5\%$ of the particle radius.

(*b*) *Test Calculations for Two Spheres Far Away from the Wall*

In principle the BEM works for arbitrary distances between the two spheres and the wall. It is important to verify that the known solutions are obtained for positions of the spheres far from the wall. Here we calculate the drag force on two equal spheres in a uniform flow. Using the same distribution and number of nodal points as before we find the force necessary to hold a mobile

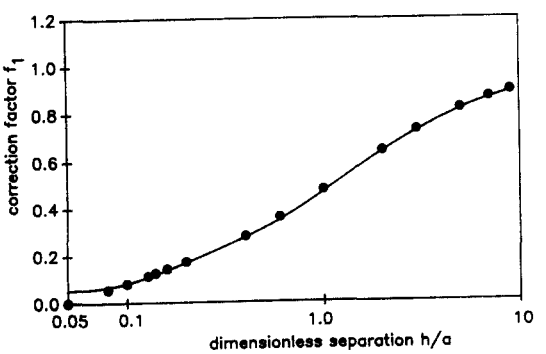

Figure 2. The drag correction factor f_1 for a spherical particle moving perpendicularly to the plane wall as a function of h/a. $f_1 = 6\pi\mu a u_z/F_z$, where u_z and F_z are the velocity and force components, respectively. ●, obtained by the BEM; ———, exact solution.

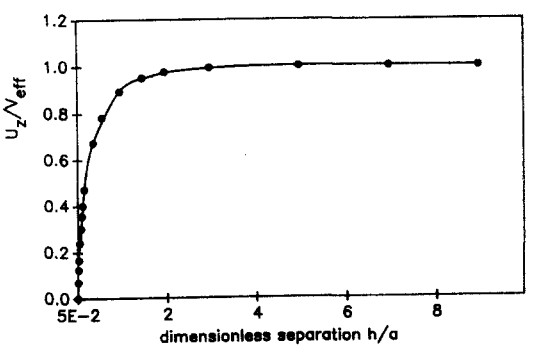

Figure 3. Normal component of the particle velocity (scaled by the fluid flow velocity at the particle center) as a function of h/a for stagnation point flow.

sphere at a given distances from the second particle, placed behind it. The force (having the same value for both spheres) can be represented as

$$\mathbf{F} = 6\pi\mu a u \lambda\left(\frac{r}{a}\right) \qquad [22]$$

where λ is the correction function to Stokes flow for a single sphere due to the presence of the second one. The results are presented in figure 5, which shows the comparison with the exact solution. In all cases the difference is $<0.5\%$, including in the limit $r \to 2$.

(c) Hydrodynamic Interactions Betweeen Two Particles Near a Solid Plane

When considering the deposition process, two effects have to be taken into account when the coating density at the solid surface is increasing: (1) the influence of the deposited particles on the flow pattern of the solution; and (2) the influence of the flowing particles on the hydrodynamic forces exerted by the fluid on a deposited particle. The first effect is responsible for all kinds of blocking effects. The second effect can result in detaching the deposited particles, if they are not adhered strongly enough to the collector surface (Varennes & van de Ven 1987). Particle blocking and detachment are responsible for the non-linear deposition kinetics frequently observed. The present method yields quantitative insight into both phenomena. Having data on the instantaneous

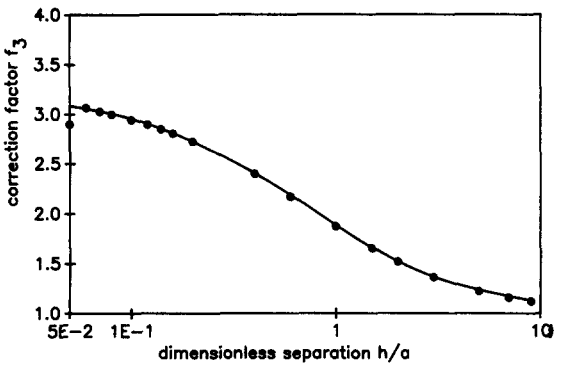

Figure 4. Drag correction factor f_2 for a stationary particle in a stagnation point flow as a function of the particle–wall dimensionless separation h/a. $f_2 = F_z/6\pi\mu A a^2 z^2$, where F_z is the normal component of the force, A being the flow intensity parameter.

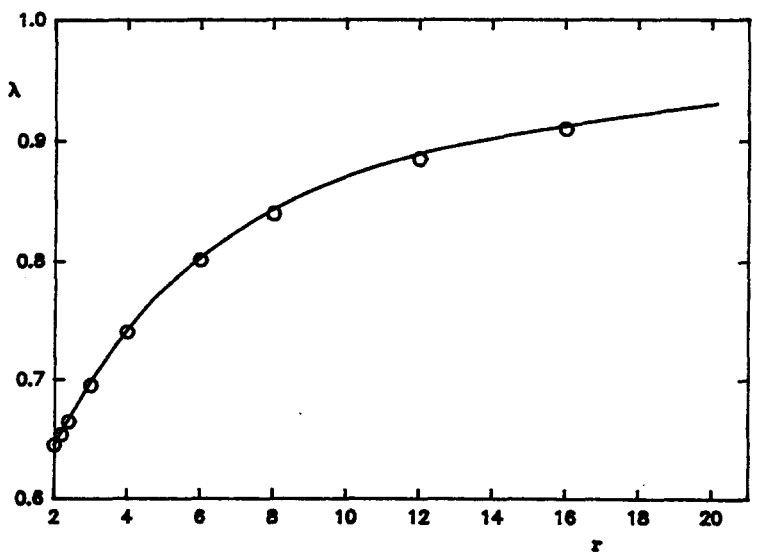

Figure 5. Drag correction for two equal spheres aligned in a uniform flow as a function of center-to-center distance.

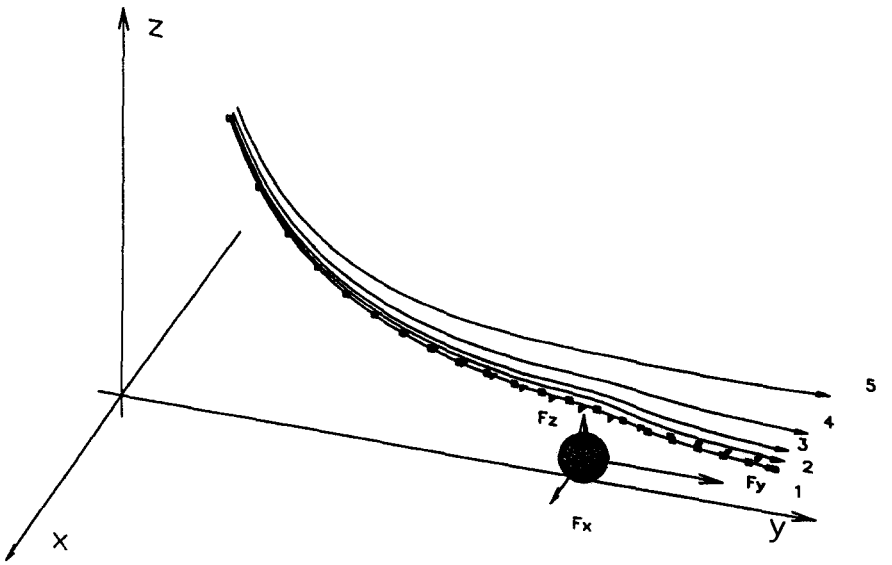

Figure 6. Trajectories of free particles in a stagnation point flow. The starting position of the particle is x_i, 4, 18), where $x_i = 0, 0.1, 0.2, 0.4$ and 0.8 for curves 1–5, respectively. The deposited particle is located at (0, 20, 1.1). □ show instantaneous positions of the particle center for a constant time interval. △ show the same for the case when the deposited particle is not present. Retardation of the movement is evident.

velocity of the particle it is possible to trace its trajectory in a given flow field. At any instant one can calculate the force and torque necessary to keep the stationary particle at a given position. In the present paper we will consider the case when the mobile particle moves freely, so no external force or torque is imposed on it. Thus, only hydrodynamic interactions are accounted for. Two external flow fields will be considered: (i) the stagnation point flow; and (ii) the plane, simple shear flow.

(i) Stagnation point flow

The flow field for this case is given by [21]. In what follows the position vectors are made dimensionless w.r.t. the particle radius a, all velocities are normalized by Aa^2 and all forces are made dimensionless to $6\pi\mu Aa^3$; A being the flow intensity parameter. Time is scaled by $1/aA$.

The stationary particle is placed at point (0, 20, 1.1). The finite distance from the wall was chosen to ensure the accuracy of the calculations, however no substantial differences are expected if the stationary particle sticks to the wall. If the freely mobile particle is far away, we calculate that the dimensionless hydrodynamic force exerted on the attached particle has components (0, 35.66, 3.55). Comparing these values with exact ones (Goren & O'Neill 1971), one can estimate the error of the calculations as 0.8%.

The freely mobile particle can be set at a given initial position and its trajectory as well as the forces on the deposited particle can be traced. Figure 6 shows the trajectories of the mobile particles starting at (x_i, 4, 18), where $x_i = 0, 0.1, 0.2, 0.4$ and 0.8. For comparison, the undisturbed trajectory at the symmetry plane in the absence of the deposited particle is shown as well. To avoid particle overlap, the free particle is pushed upwards in the collision region, but afterwards it apparently returns to the original trajectory. The squares and triangles in figure 6 show the loctions of the particles with time steps equal to 0.02. In this example the only persistent effect of the collision is a retardation of the flowing particle in its movements.

More pronounced effects are noted when the forces necessary to keep a stationary particle in a given position during the collision are considered. Figure 7 shows how the force components vary when the flowing particle passes by. For small separations the attached particle is pushed toward the wall or pulled away from it, depending on whether the freely mobile particle is in front or behind it. These results are in quantitative agreement with data shown by Dabros (1989), where calculations were done using the multisubunit method; however, only results for given two-particle configurations were presented.

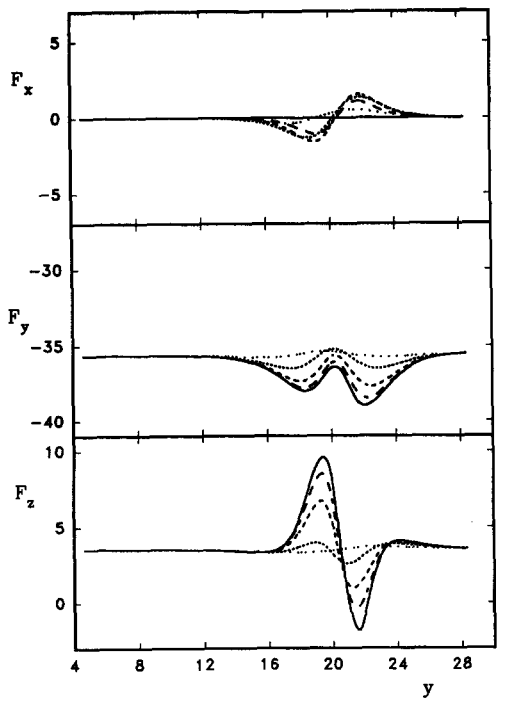

Figure 7. Force components acting on the deposited particle as a function of the y-coordinate of the flowing particle; the 5 curves (ranging from solid to dotted lines) correspond to trajectories 1–5 in figure 6, respectively. Forces are made dimensionless w.r.t. $6\pi\mu a^3 A$.

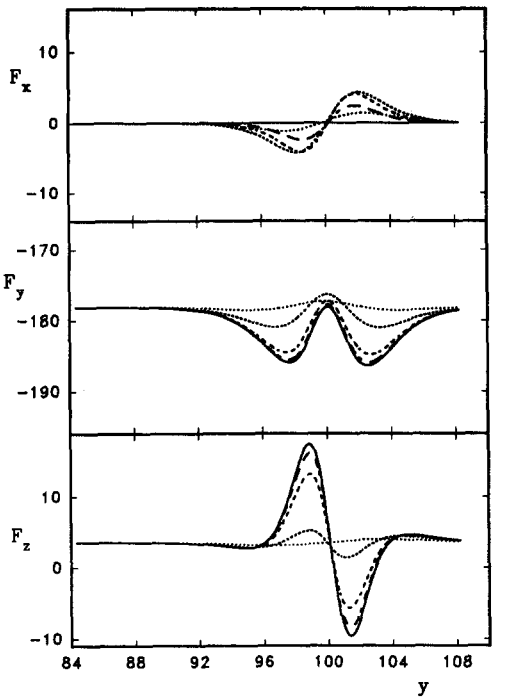

Figure 8. Force components acting on a particle deposited at (0, 100, 1.1) as a function of the y-coordinate of the flowing particle. Initial positions of the flowing particle are (x_i, 84, 4.28) for the 5 curves (ranging from solid to dotted lines). The force is made dimensionless w.r.t. $6\pi\mu a^3 A$.

Figure 8 shows the variations in the force components exerted on a stationary particle placed further away from the stagnation point ($y = 100$) when the free particle flows by. The starting position of the particle was the same as in the case discussed above. The relative variations in the tangential force are not as big as they are for the normal force. The tangential force increases when the free particle is in front or behind the deposited one. When it is straight above it, a local minimum appears.

The dependence of the torque on a stationary particle on the position of a flowing one is more complicated and even less pronounced than for the tangential force, except for configurations when the particles get very close to each other. Then the torque increases considerably.

(ii) Simple shear flow

The calculations were done for a plane, simple shear flow given by

$$v_x^0 = 0, \quad v_y^0 = z, \quad v_z^0 = 0. \qquad [23]$$

In this case, all velocities and forces were normalized w.r.t. Ga and $6\pi\mu a^2 G$, respectively. The time is scaled by G^{-1}. Figure 9 shows how the components of the force vary when the free particle is in the vicinity at a given separation from the wall. Figure 9 presents data for particular configurations of the two spheres only: in all cases the z-component of the first particle is kept constant at 1.4. The open triangles in figure 9 show results obtained by the multisubunit method described by Dabros (1989). Good agreement is noted for separations larger than a fraction of the particle dimensions.

Figure 10 shows the trajectories of a freely mobile particle and figure 11 the tangential and normal force components on the immobile particle for the case when the free particle, originally placed at point (x_i, -8, 3.1), where $x_i = 0$, 0.5, 1.0, 2.0 and 4.0, passes by the stationary one located at point (0, 0, 1.1).

As one can see, for a simple shear flow also the free particle can considerably influence the force exerted on a stationary particle.

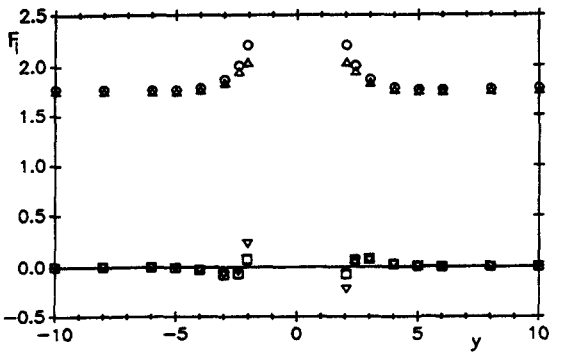

Figure 9. Dimensionless force acting on a deposited particle in a simple shear flow as a function of the position of the free particle. The stationary particle is located at the point (0, 0, 1.1). The free particle is located on the line $x = 0$, $z = 1.4$. ○ and △ show the tangential force calculated by the BEM and the multisubunit method, respectively. The □ and ▽ show similar results for the normal force.

Figure 12 shows how the force varies for different initial particle wall separations of the freely mobile particle.

DISCUSSION AND CONCLUDING REMARKS

The BEM described in this paper proved to be useful for the analysis of hydrodynamic interactions between two particles in the vicinity of a solid wall. The calculations were done for a quiescent fluid and for two external flows; namely, for the stagnation point flow and for the plane, simple shear flow. In order to speed up the calculations, in most cases 32 surface elements were used to approximate the spherical shape of the particles and 18 nodal points were applied for the force density approximation. The accuracy of the method turned out to be of the order of 1% when the particles were more than 10% of the particle radius away from the surface and apart from each other. In the wall region, fairly accurate results were obtained even below 10% of the particle radius. However, in such a case double-precision arithmetic and high-order Gaussian quadrature had to be used.

In principle, the BEM can be made as accurate as one wishes at the expense of computing time. The presented algorithm was not optimized by using, for example, adaptive grids or Gaussian quadrature order. Compared to other methods which have been or can be used to analyze similar

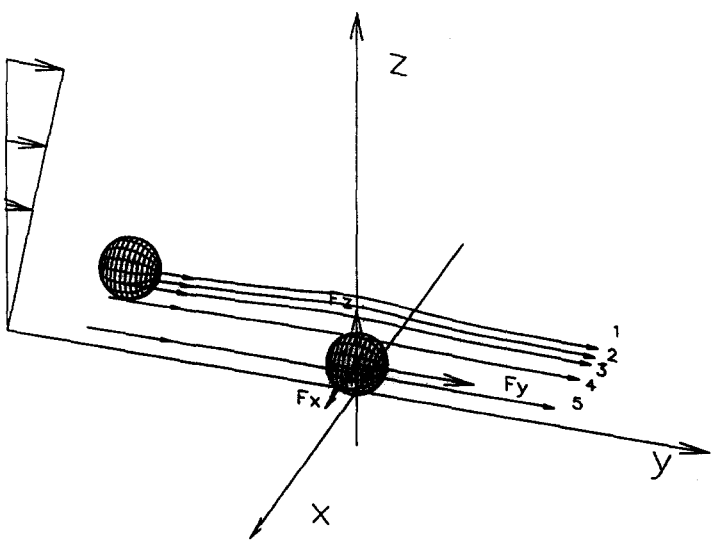

Figure 10. Trajectories of the freely mobile particle in a simple shear flow, initially located at $(x_i, -8, 3.1)$, where $x_i = 0$, 0.5, 1, 2 and 4 for curves 1–5, respectively. The deposited particle is located at (0, 0, 1.1).

problems, the BEM proved to be somewhat more accurate than the singularity (Dabros 1985) and the multisubunit methods (Dabros 1989) in the wall region. However, it is much slower, especially compared to the latter method. The boundary integral method (Hsu & Gantos 1989), used for studying the hydrodynamic interactions in the wall region of non-spherical particles, gave correct results for separations of the order 1/10 of the particle dimensions. It is not immediately obvious how the method would perform for two particles. The combination of the reflection method with lubrication theory, as presented in Malysa *et al.* (1984), is another promising alternative—in view of successful applications of a similar approach in the case of an unbounded fluid (Durlofsky & Brady 1987).

The method presented here can be useful for the analysis of the behavior of particles in colloidal systems, except for specific situations in which the colloidal interactions are of too short a range.

Results for two particles in a stagnation point flow are consistent with data obtained by a different method (Dabros 1989). The trajectory of the free particle was traced and a strong hydrodynamic interaction with the deposited particle during a "collision" was noted. This type of interaction is likely to be responsible for removal of weakly-bound particles, which were observed to detach faster when subjected to surface collisions (Varennes & van de Ven 1987). These experimental observations were for 3 μm spheres subjected to wall shear rates in the range 100–1000 s^{-1}. According to figures 11 and 12, the normal force acting on a deposited particle is about $1.2\pi\mu Ga^2$. The adsorption energy is usually in the range 1–20 kT. For an energy of β kT, the critical shear rate at which particles are removed "instantaneously" from the surface during a surface collision is $G_{crit} \simeq \beta\ \mathrm{kT}/1.2\pi\mu a^2 h$, where h is the distance at which the bond between the particle and the wall is broken. For $\beta \simeq 10$, $h \simeq 5$ nm and $a = 1.5\ \mu$m, $G_{crit} \simeq 1000\ s^{-1}$. This corresponds closely to the observed extrapolated shear rate ($G_{crit} \simeq 1650\ s^{-1}$) at which the escape time approaches zero. At lower shear rates, surface collisions result in an appreciable reduction in the escape time (equivalent to the average lifetime of a particle on the surface). At shear rates one-tenth of G_{crit}, surface collisions can reduce the escape time from 300 to 40 min. In general, the

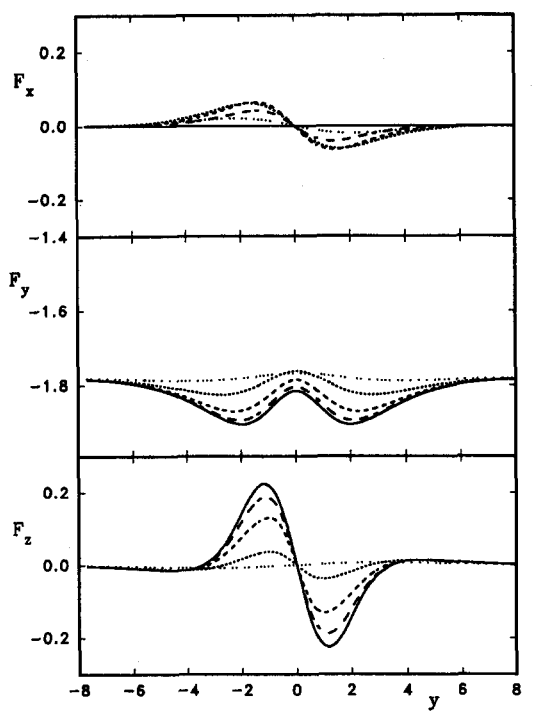

Figure 11. Force components acting on the deposited particle as a function of the y-coordinate of the flowing particle. The ———, — — —, — —, --- and ···· curves correspond to trajectories 1–5 in figure 10, respectively. Forces are made dimensionless w.r.t. $6\pi\mu a^2 G$.

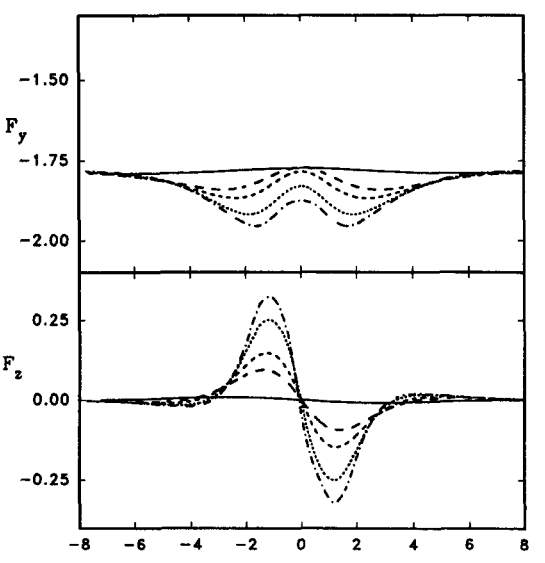

Figure 12. Force components acting on the deposited particle located at (0, 0, 1.1) in a simple shear flow as a function of the y-coordinate of the freely moving particle initially located at (0, −8, z_i), where z_i is equal to 2.8, 3, 3.5, 4 and 8 for ····, ---, — —, ——— and ——— curves, respectively. The force is made dimensionless w.r.t. $6\pi\mu a^2 G$.

normal hydrodynamic force can be important for micron-sized particles at shear rates above $100\ s^{-1}$. For smaller particles or adsorbed macromolecules, this force appears to be too weak to affect the detachment kinetics.

In the absence of colloidal interparticle forces, disturbances of the free particle trajectory are evident only in the collision region. Such disturbances are unlikely to be responsible for extensive blocking effects. It appears that colloidal forces between freely mobile and immobilzied particles are mainly responsible for the large blocking effects observed experimentally. These effects are presently being investigated.

Acknowledgements—The authors wish to thank NSERC and ICST for partial support.

REFERENCES

ADAMCZYK, Z. 1989a Particle transfer and deposition from flowing suspensions. *Colloids Surfaces* **35,** 283–308.

ADAMCZYK, Z. 1989b Particle depoosition from flowing suspensions. *Colloids Surfaces* **39,** 1–37.

ADAMCZYK, Z. & VAN DE VEN, T. G. M. 1981a Deposition of particles under external forces in laminar flow through parallel-plate and cylindrical channels. *J. Colloid Interface Sci.* **80,** 340–356.

ADAMCZYK, Z. & VAN DE VEN, T. G. M. 1981b Deposition of Brownian particles onto cylindrical collectors. *J. Colloid Interface Sci.* **84,** 497–518.

BESKOS, D. E. (Ed.) 1987 *Boundary Element Method in Mechanics.* North-Holland, Amsterdam.

BLAKE, J. R. 1971 The image system for a Stokeslet in a no-slip boundary. *Proc. Camb. Phil. Soc.* **70,** 303–310.

BOWEN, B. D. & EPSTEIN, N. 1979 Fine particle deposition in smooth parallel-plate channels. *J. Colloid Interface Sci.* **72,** 81–97.

BREBBIA, C. A., TELLES, J. C. F. & WROBEL, L. C. 1980 *Boundary Element Techniques.* Springer Verlag, Berlin.

BRENNER, H. 1961 On the slow motion of a sphere through a viscous fluid towards a plane surface. *Chem. Engng Sci.* **16,** 242–264.

DABROS, T. 1985 A singularity method for calculating hydrodynamic forces and particle velocities in low-Reynolds-number flows. *J. Fluid Mech.* **156,** 1–21.

DABROS, T. 1989 Interparticle hydrodynamic interactions in deposition processes. *Colloids Surfaces* **39,** 127–141.

DABROS, T. & ADAMCZYK, Z. 1979 Noninertial transfer to the rotating disc under an external force field (laminar flow). *Chem. Engng Sci.* **34,** 1041–1049.

DABROS, T. & VAN DE VEN, T. G. M. 1983 A direct method for studying particle deposition onto solid surfaces. *Colloid Polym. Sci.* **261,** 694–707.

DABROS, T. ADAMCZYK, Z. & CZARNECKI, J. 1977 Transport of particles to a rotating disk surface under an external force field. *J. Colloid Interface Sci.* **62,** 529–541.

DURLOFSKY, L. & BRADY, J. F. 1987 Dynamic simulation of hydrodynamically interacting particles. *J. Fluid Mech.* **180,** 21–49.

GOLDMAN, A. J., 1966 Investigations in low Reynolds number fluid-particle dynamics. Ph.D Thesis, New York Univ.

GOLDMAN, A. J., COX, R. G. & BRENNER, H. 1967 Slow viscous motion of a sphere parallel to a plane wall—I. Motion through a quiescent fluid. *Chem. Engng Sci.* **22,** 637–651.

GOREN, S. L. & O'NEILL, M. E. 1971 On the hydrodynamic resistance to a particle of a dilute suspension when in the neighborhood of a large obstacle. *Chem. Engng Sci.* **26,** 325–338.

HAPPEL, J. & BRENNER, H. 1965 *Low Reynolds Number Hydrodynamics.* Prentice-Hall, Englewood Cliffs, NJ.

HSU, R. & GANTOS, P. 1989 The motion of the rigid body in viscous fluid bounded by a plane wall. *J. Fluid Mech.* **207,** 29–72.

KIM, S. & KARRILA, S. J. 1991 *Microhydrodynamics, Principles and Selected Applications.* Butterworth-Heinmann, Boston, MA.

MALYSA, K., DABROS, T. & VAN DE VEN, T. G. M. 1984 Hydrodynamic two-sphere interactions at a wall. Report PGRLR 304, Paprican, Pointe Claire, Canada.

MALYSA, K., DABROS, T. & VAN DE VEN, T. G. M. 1986 The sedimentation of one sphere past a second attached to a wall. *J. Fluid Mech.* **162,** 157–170.

MAUDE, A. D. 1961 End effects in a falling-sphere viscometer. *Br. J. Appl. Phys.* **12,** 293–305.

OSEEN, C. W. 1927 *Hydrodynamik.* Akademische Verlagsgesellschaft, Leipzig.

PRIEVE, D. C. & RUCKENSTEIN, E. 1974 Effect of London forces upon the rate of deposition of Brownian particles. *AIChE Jl* **20,** 1178–1187.

SPIELMAN, L. A. & FITZPATRICK, J. A. 1973 Theory of particle collection under London and gravity forces. *J. Colloid Interface Sci.* **42,** 607–623.

STOKES, G. G. 1851 On the effect of internal friction of fluids on the motion of pendulums. *Trans. Camb Phil. Soc.* **9,** 8–106.

VARENNES, S. & VAN DE VEN, T. G. M. 1987 Deposition and detachment of latex particles at glass surfaces exposed to flow. *PhysicoChem. Hydrodynam.* **9,** 537–559.

VAN DE VEN, T. G. M. 1989 *Colloidal Hydrodynamics.* Academic Press, London.

WEINBAUM, S., GANATOS P. & YAN, Z. Y. 1990 Numerical multipole and boundary integral equation techniques in Stokes flow. *A. Rev. Fluid Mech.* **22,** 275–316.

YOUNGREN, G. K. & ACRIVOS A. 1975 Stokes flow past a particle of arbitrary shape: a numerical method of solution. *J. Fluid Mech.* **69,** 377–403.

APPENDIX

Equation [19] can be rewritten in the following form:

$$\begin{bmatrix} A^1_{6,3M} & \vdots\ 0 & \vdots\ 0 \\ \cdots & \cdots & \cdots \\ & \vdots & \vdots\ A^3_{6,3M} \\ A^2_{6M,6M} & \vdots & \vdots\ \cdots \\ & \vdots & \vdots\ 0 \end{bmatrix} \cdot \begin{bmatrix} f^1_{3M} \\ \cdots \\ f^2_{3M} \\ \cdots \\ u^i_6 \end{bmatrix} = \begin{bmatrix} F^1_6 \\ \cdots \\ V^1_{3M} \\ \cdots \\ V^2_{3M} \end{bmatrix}. \qquad [A.1]$$

The components of the vector of unknown values in [A.1] are:

(i) $3M$ force components acting at M nodal points of the first (mobile) sphere $f^1_{3M} = ({}^1f^1_1, {}^1f^1_2, {}^1f^1_3, \ldots, {}^1f^M_3)$;
(ii) $3M$ force components acting at the nodal points of the second (stationary) sphere $f^2_{3M} = ({}^2f^1_1, {}^2f^1_2, {}^2f^1_3, \ldots, {}^2f^M_3)$; and
(iii) three translational and three rotational velocity components of the first particle denoted by $u^1_6 = ({}^1u_1, {}^1u_2, {}^1u_3, {}^1\omega_1, {}^1\omega_2, {}^1\omega_3)$.

The right-hand side vector of [A.1] consists of:

(i) three components of the force and three components of the torque acting on the first partice $F^1_6 = ({}^1F_1, {}^1F_2, {}^1F_3, {}^1T_1, {}^1T_2, {}^1T_3)$;
(ii) $3M$ components of the external fluid velocity at nodal points of the first particle V^1_{3M}; and
(iii) $3M$ components of the external fluid velocity at nodal points of the second particle, V^2_{3M}.

The elements of matrix A are derived from [11]–[13] making use of [14], [16] and [17].

The first three rows of the submatrix $A^1_{6,3M}$ can be found from [12], which can be, more explicitly, rewritten in an index form as

$$\sum_{\beta\gamma} {}^1f^\gamma_i \int_\beta N^\gamma(\eta_1, \eta_2)|J|\, d\eta_1\, d\eta_2 = {}^1F_i, \qquad [A.2]$$

where ${}^{1}F_i$ is the $i(i = 1, 2, 3)$ component of the external force acting on the mobile particle and ${}^{1}f_i^{\gamma}$ is the component of the force density at the node γ of the surface element β of the particle. N^{γ} and $|J|$ are the shape function and the transformation Jacobian, respectively. The sum of integrals, appearing in the equation, over the γ index is equal to the corresponding coefficient of the submatrix.

The next three rows of the submatrix can be determined in a similar fashion from [13], which can be written as

$$\sum_{\alpha\beta\gamma jk} f_k^{\beta} \epsilon_{ijk} r_j^{\alpha} \int_{\beta} N^{\alpha}(\eta_1, \eta_2) N^{\beta}(\eta_1, \eta_2) |J| \, d\eta_1 \, d\eta_2 = {}^{1}T_i, \qquad [A.3]$$

where $i, j, k = 1, 2, 3$ and α, β, γ depend on the order of the interpolation function $N^{\beta}(\eta_1, \eta_2)$; r_j^{α} is the j component of the local vector pointing from the center of the particle to the nodal point α; ϵ_{ijk} is the fully antisymmetrical tensor. Elements of the submatrix $A^2_{6M,6M}$ are calculated from [11], which can be written for $2M$ nodal points $\mathbf{x}$ of both spheres:

$$-\sum_{jkn\beta\gamma} {}^{n}f_j^{\gamma} \int_{\beta} G_{ij}(\mathbf{x}, \mathbf{y}(\eta_1, \eta_2) N^{\gamma} |J| \, d\eta_1 \, d\eta_2 + {}^{n}u_i + \epsilon_{ijk} {}^{n}\omega_j r_k = v_i^0(\mathbf{x}), \qquad [A.4]$$

where $n = 1, 2, \quad i, j, k = 1, 2, 3$ and ${}^{n}u_k$ and ${}^{n}\omega_k$ are the components of the particle translational and angular velocity, equal to zero for the second particle.

The integrals appearing in [A.2]–[A.4] were calculated by the Gauss method of integrating over triangular surface elements. If the nodal point belongs to the element over which integration is carried out a special method has to be used, as indicated in the text, to minimize the errors.

The submatrices under consideration are determined by values of the integral over the surface elements to which the nodal points belong. It is thus necessary to define a grid structure of the nodal points distributed over the surfaces.

The submatrix $A^3_{6,3M}$ is related to the last two terms of the left-hand side of [A.3]. Elements of the first three columns of the submatrix are equal to δ_{ij} (δ_{ij} being the Kronecker delta), where i indicates the actual component of the external velocity in the matrix row and j is the submatrix column index.

The last three columns of the submatrix are equal to $\Sigma_k \epsilon_{ijk} r_k$, where $k = 1, 2, 3$. In this case i has the same meaning as previously and j indexes the last three columns of the submatrix $A^3_{6,3M}$.